ACS Photonics

Letter

pubs.acs.org/journal/apchd5

Polymer Photonic Crystal Nanocavity for Precision Strain Sensing

Xuetao Gan,*[,†] Hannah Clevenson,[‡] and Dirk Englund*[,‡]

[†]School of Science, Northwestern Polytechnical University, Xi'an 710072, China

[‡]Department of Electrical Engineering and Computer Science, Massachusetts Institute of Technology, Cambridge, Massachusetts 02139, United States

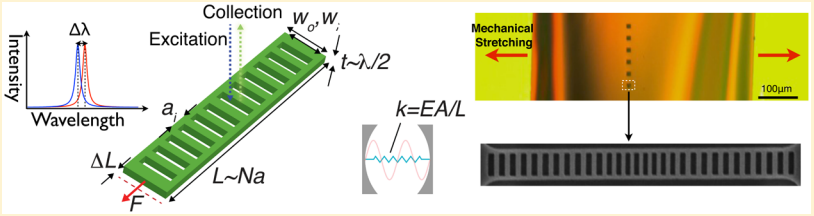

ABSTRACT: We propose and experimentally demonstrate flexible one-dimensional polymer photonic crystal nanocavities with quality factors exceeding 10^4 for precision sensing of strain at experimentally measured values of 10^{-4}. Relying on the cavity's compact structure and polymer's low Young's modulus, the cavity's displacement and the applied force are estimated as 0.94 nm and 55 nN, respectively. This flexible-nanocavity microsensor shows high linearity and repeatability. The microsensor concept is also compatible with liquid environments. The ease of fabrication, flexibility, and biocompatibility of the polymer microsensor promise applications in strain and force measurements at the microscale in the physical, material, and life sciences.

KEYWORDS: *polymer photonics, photonic crystal cavity, strain sensing, precision sensing*

Strain, displacement, and force sensors are used across a wide range of fields, from the characterization of individual molecule forces[1,2] to precision motion control to gravitational wave detection.[3] Recently, sensitive force sensors were demonstrated based on microelectromechanical,[4−6] nano-optomechanical,[7] and atomic force microscopy.[8,9] Here, we report on a new type of displacement sensor based on a suspended polymer photonic crystal (SPPC) nanocavity[10,11] with subwavelength light confinement and high quality (Q) factors exceeding 12000. An embedded green dye internally illuminates the cavity resonance, producing a sharp line in the visible spectrum. These devices, which are fabricated in the prevalent polymer polymethyl-methacrylate (PMMA), form stand-alone sensors that can be monitored remotely using only optical spectroscopy. Compared to other optical force sensors such as an atomic force microscope, the cavity resonance amplifies the targeted displacement in proportion to the cavity finesse, which is proportional to Q/V, where V is the mode volume. This microsensor detects a strain of 10^{-4} via shifts in the resonance wavelength, which also indicates a subnanometer displacement and nanonewton force sensor considering the compact cavity structure and low Young's modulus of the polymer material. The PMMA, which is itself an electron beam lithography resist, eliminates typical mask-transfer steps, promising straightforward and reproducible device fabrications. In addition, the SPPC cavity promises high Q resonant modes even in an aqueous environment, which could extend the microsensor's applications in biochemical samples combining with PMMA's biocompatibility.

As illustrated in Figure 1a, the polymer cavity is based on a one-dimensional (1D) ladder design similar to that used in high-index solids,[12−14] but optimized for the lower index contrast between PMMA (with the refractive index of ∼1.5) and air, with a central lattice defect produced by a parabolic variation in the lattice constants. If a force F applied across the ladder cavity of length L stretches it by a small distance ΔL, the fractional cavity resonance shift follows the cavity strain, $\Delta\lambda/\lambda = \Delta L/L$. We monitor the optical signal from the cavity by measuring the reflectivity of an external input light or the emission from an internal light source in the cavity.

Finite element simulations (COMSOL Multiphysics) enable an estimation of the ladder deformation as the film is stretched along the ladder beam. Figure 1b shows the predicted strain of the ladder cavity, where the black frame and colormap represent the original geometry and deformed structure of the ladder cavity, respectively. Comparing the widths of the original and deformed structures, we see no noticeable transverse deformation. All deformation is longitudinal along the length of the ladder cavity. Figure 1b also plots the displacement (Δx) along the middle of the ladder beam (x), and the inset shows displacements of the lattice spacing between two adjacent holes (Δa). The displacement difference of two adjacent holes are nearly identical with a deviation range of 0.6%, indicating that the lattice spacing of the ladder stretches uniformly. The simulation also confirms the rectangular holes of the ladder beam have no observable deformation if the strain is not high (smaller than 0.02).

For the case of weak deformation (with strain smaller than 0.02), according to the photonic band theory in photonic

Received: February 28, 2017
Published: June 23, 2017

DOI: 10.1021/acsphotonics.7b00030
ACS Photonics 2017, 4, 1591−1594

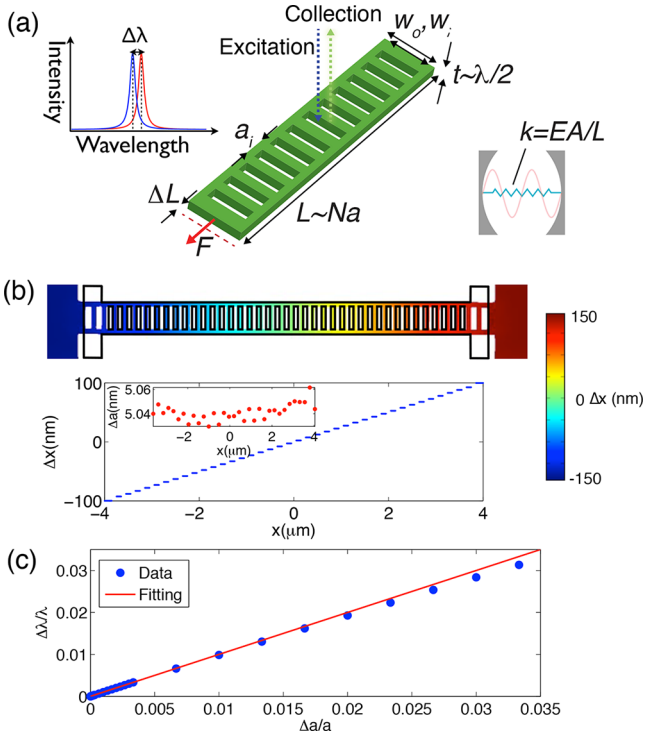

Figure 1. (a) Schematic of the SPPC microsensor. The ladder has a length of L and is stretched by an external force F, which causes a total displacement of ΔL. The resonant wavelength of the cavity shifts by $\Delta\lambda$ when this force is applied. The optical signal from the nanocavity is monitored by measuring the reflectivity of an external input light or the emission of an internal light source in the cavity. (b) Simulation result of the mechanical deformation of the ladder cavity with a longitudinal stretch along the beam. (c) Simulated resonant wavelength shift $\Delta\lambda/\lambda$ with respect to the strain $\Delta a/a$.

crystals, the strain ξ on one lattice period corresponds to the resonant wavelength shift as follows: $\xi = \Delta a/a \approx \Delta\lambda/\lambda_0$, where Δa is the extension of the lattice constant a, and λ_0 is the resonant wavelength of the unloaded cavity. Next, we derive the quantities $\Delta L = L\xi = L\Delta\lambda/\lambda$ and $F = EA\xi = EA\Delta\lambda/\lambda_0$, where E is the Young's modulus of the polymer and A is the cross-section area of the ladder. Therefore, the strain and displacement over the ladder cavity follow linearly the resonant wavelength shift. We used the finite element model to confirm this linear relationship (using COMSOL's Structural Mechanics and RF modules), as shown in Figure 1c. A deviation from the linear fitting presents for the strain larger than 0.02 because of the deformations of the rectangle air holes. A wavelength shift of $\Delta\lambda_{min}$ produces a clearly observable cavity shift when it equals cavity resonance linewidth, λ_0/Q. Averaging over many cavity photons may reduce this detectable shift, depending on the underlying noise sources, as described below.

We developed the high Q SPPC ladder cavity with the following optimized designs: thickness of the photonic crystal slab $t = 1.4a$, beam width $w_0 = 2.8a$, hole width $a_2 = 0.52a$, and hole height $w_1 = 0.84w_0$.[11] The cavity defect region consists of a parabolically decreasing lattice spacing to $0.9a$ at the center over five periods to avoid an impedance mismatch between the waveguide mode and the lattice Bloch mode.[15] An optimized resonant mode of the cavity has a Q factor of 107000 at the normalized wavelength $a/\lambda = 0.447$ and a mode volume (V_{mode}) of $1.36(\lambda/n)^3$. This record-small V_{mode} for a polymer resonator enables the high sensitivity to displacement in the cavity region. The top of Figure 2a shows the energy field distribution of the resonance. Remarkably, it is possible to obtain a moderately high Q factor of 2100, even when the polymer cavity is surrounded by an index of 1.33 (water). The energy field distribution is displayed in the bottom of Figure 2a, showing increased evanescent field in surrounding region than that seen in the air environment. This moderately high Q resonant mode in an aqueous environment could extend applications of the microsensor to biomedical and tissue engineering.

The PMMA-based nanocavities can be designed to have high-Q factor resonances across a wide spectral range within the material's wide transparency range. In this work, we design the nanocavities to be resonant in the visible spectral range, allowing for the detection of optical signal using commonly available silicon photodetectors. We fabricated the SPPC ladder cavities with a lattice spacing a between 265 and 285 nm. We exposed the patterns using electron beam lithography on a 400 nm thick PMMA layer, which is applied to a silicon substrate via spin-coating with a 10 nm poly(vinyl alcohol) (PVA) spacer layer. When the chip is immersed in water, the water-soluble PVA layer enables the lift-off of the developed PMMA film from the substrate. The patterned PMMA film floats to the surface of the water, where it is easily transferred onto a carrier structure with gaps to suspend the cavities. Because this process eliminates the typical mask transfer steps used for semiconductor photonic crystals, the ladder cavity shows excellent spatial resolution, as shown in the scanning electron microscope image in Figure 2b. Figure 2c shows an optical image of a finished sensor device. To test strain sensing with these polymer cavities, we suspended the PMMA film with ladder cavities across a ~320 μm wide air-gap of a mechanical carrier. One side of the air-gap carrier is connected to a piezo-actuated stage and moves freely to stretch the ladder cavities. The

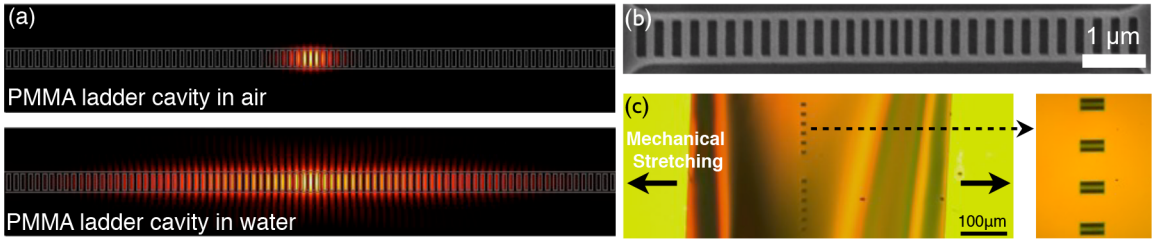

Figure 2. (a) Energy field distributions of the simulated resonant modes of the designed SPPC cavity in air (top) and water (bottom) environments, respectively. (b) Scanning electron microscope image of the suspended ladder nanocavity. (c) Optical microscope image of the nanocavity-based displacement sensor. The PMMA film with ladder cavities is suspended on a mechanical carrier, which is connected to a piezo-actuated stage to stretch the flexible cavities.

DOI: 10.1021/acsphotonics.7b00030
ACS Photonics 2017, 4, 1591−1594

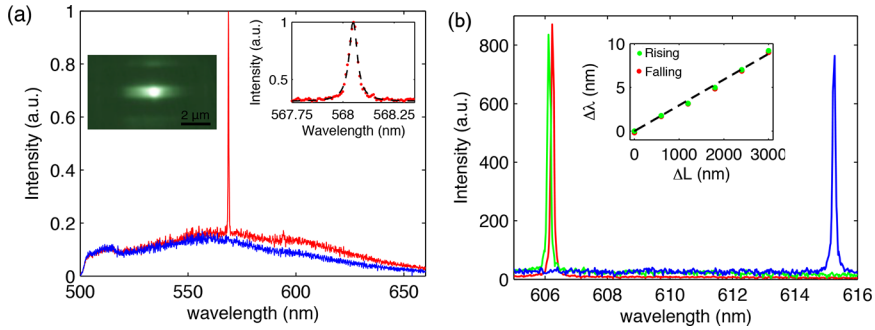

Figure 3. Characterization of the nanocavity-based displacement sensor. (a) Spectra of the PL emission from the defect section of the cavity, where the red and blue curves correspond to spectra acquired under orthogonal polarizations. The linearly polarized cavity mode represents a high and narrow peak at the wavelength of 568.1 nm. Left inset displays the PL image of the cavity, showing a bright spot at the defect center. Right inset shows the Lorentizan fitting on the cavity mode, indicating a Q factor of 12000. (b) Spectra acquired from the device with different stretching forces, where the green and red curves give the smallest distinguished displacement and the blue curve shows the maximum displacement. Inset gives the bidirectional sampling of the device showing linearity, where the green and red dots represent the resonant wavelength shifts with the stretching and releasing of the polymer film.

position of the stage is controlled precisely by a close-loop system and has a resolution of 5 nm.

With the sample mounted, we measured the cavity wavelength response under a confocal microscope setup. To simplify these measurements, we doped the PMMA with an organic dye (Coumarin 6, 5% by weight) to serve as an internal light source with photoluminescence (PL) around the wavelength range of 480−650 nm. A 405 nm diode laser focused onto the cavities produced strong PL emission that we analyzed using a 0.5 m spectrometer. The left inset of Figure 3a shows the bright PL emission from the cavity, indicating a cavity-enhanced emission of the organic dye.[10] The blue and red curves displayed in Figure 3a show the collected PL spectra for two orthogonal polarizations (along and orthogonal to the cavity axis). This measurements shows the cavity-enhanced emission at the resonance wavelength of 568.1 nm, which has a Q factor higher than 12000 determined by a Lorentizan fit (as shown in the right inset of Figure 3a). The corresponding line width is at the limit of our spectrometer, so the Q value of 12000 represents a lower bound. The resonant modes of other ladder cavities in the suspended film were characterized as well, showing Q factors higher than 10^4 and resonant wavelengths ranging between 550 and 610 nm. To our knowledge, these suspended nanocavities show the highest Q factor in the visible spectral range in polymer resonators.

The high Q factor and flexible material of these photonic crystal nanocavities allow for precision sensors of strain in response to an applied longitudinal force. Figure 3b summarizes these strain measurements as a nanocavity with unloaded resonance at 606.1 nm and Q factor of 11000 is stretched. As the piezo stage is moved in increments of 30 nm, the cavity red-shifts in steps of ∼0.06 ± 0.005 nm (from green peak to the red peak in Figure 3b), where the estimated uncertainties are near those expected for shot noise from our spectrometer. While the ∼320 μm wide PMMA film has several microscale ladder cavities, for the moderately weak deformation (with strain smaller than 0.02), the strain over the whole suspended PMMA film is uniform, as indicted by the finite element simulation result. The strain over the ladder beam can therefore be approximated by $\xi = 0.03/320 \approx 94 \times 10^{-6}$. According to the theoretical curves demonstrated in Figure 1, this strain would induce a resonance wavelength shift of $\lambda_0\xi \approx 0.057$ nm, which is approximately a cavity fwhm line width and therefore within the measurement uncertainty. Considering the length of the cavity is ∼10 μm, these experiments indicate a cavity resonance shift by a whole line width for a displacement of only ∼0.94 nm.

Because of PMMA's low Young's modulus of E = 1.8 GPa, and the cavity's very small cross section of A = 0.32 μm^2, these experimental measurements indicate that a single cavity is sensitive to a force of only $F = EA\xi \approx 55$ nN before signal averaging. With the microstage moved by a maximum displacement of 5 μm, the resonant wavelength shifts by a 9.2 nm with almost no variations of the peak intensity and Q factor, as shown in the blue peak in Figure 3b. We also examine the linearity and repeatability of the sensor by increasing and decreasing the air-gap gradually. The resonant wavelength shifts of the ladder cavity versus the displacements of the microstage are plotted in the inset of Figure 3b. The bidirectional sampling results show that both the rising and falling sides are nearly linear with low hysteresis.

The above estimations of the sensitivities are made by assuming a whole resonance line width shift is necessary in the PL spectrum. Assuming shot-noise limited detection of n signal photons from cavity transmission or photoluminescence, cavity shifts below the line width could be resolved to achieve, in principle, a minimum strain of order $1/Q \cdot 1/\sqrt{n}$. Even for $n \sim 1$, this corresponds to a small strain of $\sim 10^{-4}$, or about 1 nm for our ∼10 μm long cavity. However, photon shot noise may not be the dominant noise source in the relevant detection bandwidth. In particular, another important noise component is due to thermal motion at a finite environment temperature. At thermal equilibrium, the equipartition theorem gives $k\Delta L^2/2 = k_B T/2$, indicating the thermal noise of the displacement ΔL at room temperature of T = 300 K. Here, $k = AE/L$ is the spring constant of the polymer ladder along the longitudinal direction, and k_B is the Boltzmann constant. With the geometry of the employed ladder cavity, the calculated thermal noise displacement is ∼3 pm, corresponding to measurement noises of strain and force of 3×10^{-7} and 0.17 nN. Further work is needed to carefully characterize these limits through noise spectral density measurements.

In conclusion, we introduced a 1D polymer cavity-based optical sensor for measuring strain, displacement, and force that sets new records for similarly sized devices. Relying on the high Q factor resonant mode and excellent polymer material properties, we observed one resonant line width shift of 0.06 nm, corresponding to a strain of 94×10^{-6}, and estimated

DOI: 10.1021/acsphotonics.7b00030
ACS Photonics 2017, 4, 1591−1594

displacement and force of ∼0.94 nm and 55 nN. Considering the wavelength interrogation error of 0.005 nm as the resonant wavelength variation $\Delta\lambda$ in our measurement system, it would lead to errors for strain, displacement, and force of 8.2×10^{-6}, 2.6 nm, and 4.8 nN, respectively. The practical lower limits are set by the thermal noise floor, which predicts minimum detectable displacement of ∼3 pm. One-step lithography, without the need for dry etching, allows these polymer sensors to be easily fabricated in large numbers, which are compatible with optical lithography and nanoimprinting techniques as well. It requires an almost identical amount of resources to produce a single sensor as a large array of sensors; this allows maps of strain over an area to be produced, and to perform multiple measurements in parallel, lowering the signal-to-noise ratio and providing redundancy for use in remote environments. Considering the possible high Q resonant modes of SPPC cavities in aqueous solution, this work also promise to provide new tools for biomedical applications.

AUTHOR INFORMATION

Corresponding Authors

*E-mail: xuetaogan@nwpu.edu.cn.
*E-mail: englund@mit.edu.

ORCID

Dirk Englund: 0000-0002-1043-3489

Notes

The authors declare no competing financial interest.

ACKNOWLEDGMENTS

Financial support was provided by the Air Force Office of Scientific Research PECASE, supervised by Dr. Gernot Pomrenke. FDTD simulations were carried out in part at the Center for Functional Nanomaterials, Brookhaven National Laboratory, which is supported by the U.S. Department of Energy, Office of Basic Energy Sciences, under Contract No. DE-AC02-98CH10886. H.C. was supported in part by the NASA Space Technology Research Fellowship. X.G. was partially supported by the NSFC (61522507, 11404264). D.E. acknowledges partial support from the STC Center for Integrated Quantum Materials (CIQM), NSF Grant No. DMR-1231319.

REFERENCES

(1) Wang, M.; Yin, H.; Landick, R.; Gelles, J.; Block, S. Stretching DNA with optical tweezers. *Biophys. J.* **1997**, *72*, 1335−1346.
(2) Frei, M.; Aradhya, S. V.; Hybertsen, M. S.; Venkataraman, L. Linker Dependent Bond Rupture Force Measurements in Single-Molecule Junctions. *J. Am. Chem. Soc.* **2012**, *134*, 4003−4006.
(3) Lyons, T. T.; Regehr, M. W.; Raab, F. J. Shot Noise in Gravitational-Wave Detectors with Fabry-Perot Arms. *Appl. Opt.* **2000**, *39*, 6761−6770.
(4) Basarir, O.; Bramhavar, S.; Basilio-Sanchez, G.; Morse, T.; Ekinci, K. L. Sensitive micromechanical displacement detection by scattering evanescent optical waves. *Opt. Lett.* **2010**, *35*, 1792−1794.
(5) Sun, Y.; Fry, S.; Potasek, D.; Bell, D.; Nelson, B. Characterizing fruit fly flight behavior using a microforce sensor with a new comb-drive configuration. *J. Microelectromech. Syst.* **2005**, *14*, 4−11.
(6) Muntwyler, S.; Beyeler, F.; Nelson, B. J. Three-axis micro-force sensor with sub-micro-Newton measurement uncertainty and tunable force range. *J. Micromech. Microeng.* **2010**, *20*, 025011.
(7) Li, M.; Pernice, W. H. P.; Tang, H. X. Broadband all-photonic transduction of nanocantilevers. *Nat. Nanotechnol.* **2009**, *4*, 377−382.
(8) Srinivasan, K.; Miao, H.; Rakher, M. T.; Davanço, M.; Aksyuk, V. Optomechanical Transduction of an Integrated Silicon Cantilever Probe Using a Microdisk Resonator. *Nano Lett.* **2011**, *11*, 791−797.
(9) Mamin, H. J.; Rugar, D. Sub-attonewton force detection at millikelvin temperatures. *Appl. Phys. Lett.* **2001**, *79*, 3358−3360.
(10) Gan, X.; Clevenson, H.; Tsai, C.-C.; Li, L.; Englund, D. Nanophotonic Filters and Integrated Networks in Flexible 2D Polymer Photonic Crystals. *Sci. Rep.* **2013**, *3*, 2145.
(11) Clevenson, H.; Desjardins, P.; Gan, X.; Englund, D. High sensitivity gas sensor based on high-Q suspended polymer photonic crystal nanocavity. *Appl. Phys. Lett.* **2014**, *104*, 241108.
(12) Gong, Y.; Ishikawa, S.; Cheng, S. L.; Gunji, M.; Nishi, Y.; Vučković, J. Photoluminescence from silicon dioxide photonic crystal cavities with embedded silicon nanocrystals. *Phys. Rev. B: Condens. Matter Mater. Phys.* **2010**, *81*, 235317.
(13) Eichenfield, M.; Camacho, R.; Chan, J.; Vahala, K. J.; Painter, O. A picogram- and nanometre-scale photonic-crystal optomechanical cavity. *Nature* **2009**, *459*, 550−555.
(14) Notomi, M.; Kuramochi, E.; Tanabe, T. Large-scale arrays of ultrahigh-Q coupled nanocavities. *Nat. Photonics* **2008**, *2*, 741−747.
(15) Sauvan, C.; Lecamp, G.; Hugonin, J. Modal-reflectivity enhancement by geometry tuning in photonic crystal microcavities. *Opt. Express* **2005**, *13*, 245.

DOI: 10.1021/acsphotonics.7b00030
ACS Photonics 2017, 4, 1591−1594